Prediction and Measurement of Damping of a Laminated Beam with a Constrained Viscoelastic Layer

D. J. Segalman
Applied Mechanics Division I
Sandia National Laboratories
Albuquerque, New Mexico 87185
(505) 846-1899

Lt. Philip Reamy
Air Force Weapons Laboratory/ARBC
Albuquerque, New Mexico 87117-6008
(505) 844-2019

Abstract

Analytic predictions [1] for damped natural frequencies of a simple viscoelastic structure are compared with measured values [2]. The structure studied is an aluminum channel incorporating a constrained layer of highly viscoelastic polymer. The predictive technique employs a general and systematic method for calculating damping and stiffness matrices using only measured material properties and structure geometry. These matrices are then used to predict the dynamic properties of the structure. This work constitutes the first step in the experimental verification of the analytic method.

Agreement between the predicted and measured response of the structure studied is very good, and indicating that the analytic technique used is a viable method for modeling viscoelastically damped structures.

[1]The computational portion of this work was supported by Sandia National Laboratories under contract to the U.S. Department of Energy (DE-AC04-76DP00789).

[2]The experimental portion of this work was funded under Laboratory Independent Research Program 8722 of the Air Force Weapons Laboratory.

Contents

1. Introduction

The Role and Importance of Damping

Viscoelastic damping is a traditional method of controlling vibration and noise in structures and machinery. An example of this method of passive damping is the use of high-loss grommets in the attachment of subsystems. More sophisticated applications include the use of constrained layer damping treatments to reduce vibration in airplane shells that had previously suffered fatigue damage. Yet more advanced applications have been proposed, involving coupling viscoelastic damping with active controls in space structures.

Advanced analysis methods, particularly finite element methods, can be used to predict stresses, mode shapes, and natural frequencies adequately for guidance in the design of complex elastic structures. The utility of these elastic analysis techniques has been delineated by experimental as well as theoretical means. New methods, including that of Segalman [4], have been developed to enable corresponding calculations for viscoelastic structures. The work presented here is an experimental verification of that method.

Analytic Prediction of Damping

Inducing damping response in an otherwise elastic structure through the use of constrained viscoelastic layers is a technique that has been applied since the late 1950's. The work of Ross, Ungar, and Kerwin [1] marks the beginning of meaningful analytic methods for prediction and design of damping treatments for simple structures. Such methods are generally restricted to problems of beams and flat plates, for which closed form expressions for frequency and mode shape can be derived.

A technique for addressing constrained layer damping of more general structures was developed later as the "modal energy method" [2,3]. This method employs assumptions analogous to those underlying the Ross, Kerwin, and Ungar method for beams and plates, but generalizes them to forms that can be employed with finite element solutions for frequency and deformed mode.

The above prediction methods are restricted to problems involving primarily elastic structures with distinct viscoelastic regions. There is a further restrictive assumption embedded in those methods that the damped modes are identical to corresponding elastic modes. These restrictions sufficiently limit the application of those techniques that it is necessary to examine more general methods.

One more general method for prediction of damping in linearly viscoelastic structures was proposed by Segalman [4]. That work consisted of a purely formal derivation. The purpose of the work presented below is to test a numerical implementation of that method against measurements on a very simple viscoelastic structure. The results, shown below, provide strong encouragement to the authors to address more complex structures, for which the generality of the analytic method tested here can be demonstrated.

2. Analytic Method

2.1 Formulation

Formal Evaluation of Damping and Stiffness Matrices

The method presented in [4] begins with consideration of a nearly elastic structure, possessing only a small amount of viscoelasticity. This "slightly viscoelastic" structure consists of an underlying elastic system plus small contributions from the integral terms associated with viscoelastic material response. A perturbation expansion yields formal expressions for the complex modes and frequencies of the structure. (That expansion involves the natural modes and frequencies of the underlying elastic structure, whose elastic properties are those which would be measured in quasistatic experiments.)

A perturbation expansion is also performed on a similar but slightly damped, nearly elastic structure. This "slightly damped" system consists of the same underlying elastic structure plus small perturbations in the damping and stiffness matrices. Formal expressions for the damping and stiffness matrices of the second structure are obtained by requiring that the complex modes and frequencies of the two structures agree. The formal process described above is represented by the chart of Figure 2.1.

The strategy outlined above results in the following expressions for the damping and stiffness matrices:

$$C = \sum_{\text{modes } n=1}^{N} Im\left(\frac{1}{\omega^n} \Gamma^*(\omega^n)\, x^n\, (z^n)^T \right) \tag{2.1}$$

and

$$K = \sum_{\text{modes } n=1}^{N} Re\left(\Gamma^*(\omega^n)\, x^n\, (z^n)^T \right) \tag{2.2}$$

where $\Gamma^*(\omega)$ is the complex structural stiffness matrix of the viscoelastic structure evaluated at frequency ω.

N is the number of elastic eigensolutions retained in the calculation.

and ω^n is the n'th eigenfrequency and x^n is the n'th eigenmode of the elastic structure. Together, ω^n and x^n are the n'th eigen solution to the equation:

$$\left[-(\omega^n)^2 M + K_o\right] x^n = 0 \tag{2.3}$$

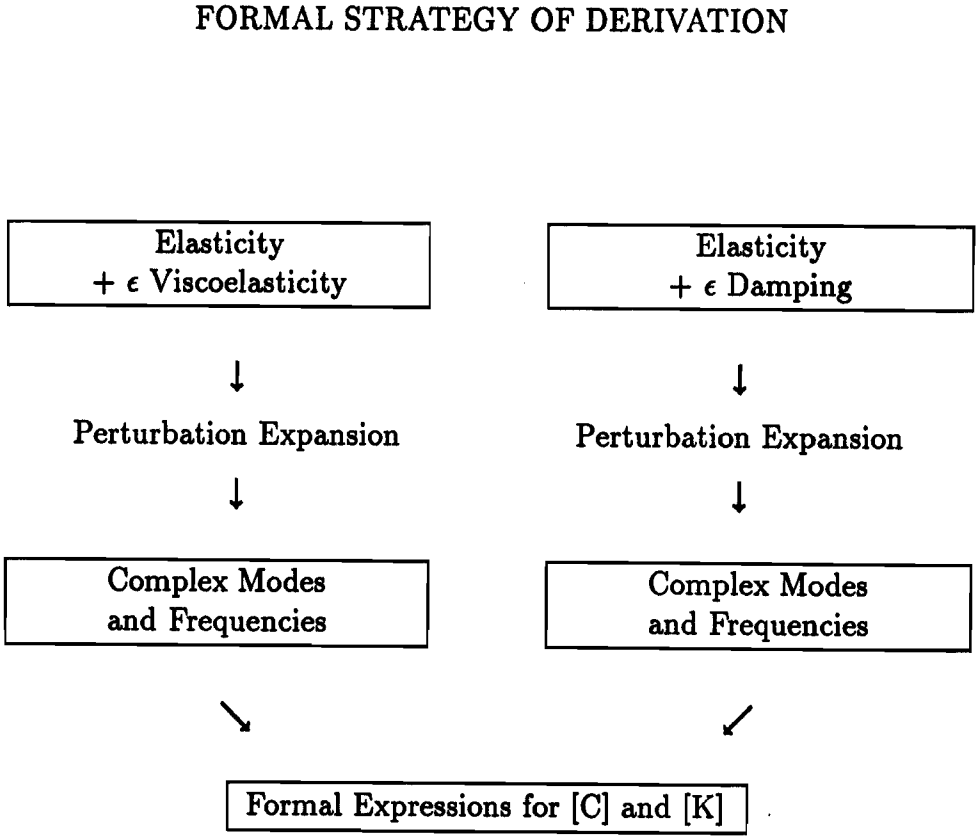

Figure 2.1. Outline of Strategy for Calculation of Damping and Stiffness Matrices for Linearly Viscoelastic Structures

The remaining quantities, z^n and K_o are defined by:

$$K_o = \Gamma^*(0) \tag{2.4}$$

$$f^n = K_o\, x^n \tag{2.5}$$

and

$$z^n = f^n \,/\, (x^n)^T f^n \tag{2.6}$$

(In Equations 2.1 and 2.2 and in what follows, expressions such as $x^n\,(z^n)^T$ are matrix-valued outer products, and expressions such as $(x^n)^T\, z^n$ are scalar-valued inner products.)

When the damping and stiffness terms are combined with inertial terms, a second order system of equations results:

$$M\,\ddot{x}(t) \;+\; C\,\dot{x}(t) \;+\; K\,x(t) = r(t) \tag{2.7}$$

where M is the structural mass matrix;
$x(t)$ is the generalized (nodal) displacement vector;
and $r(t)$ is the corresponding force vector.

Some observations should be made at this point.

- The complex stiffness matrices $\Gamma^*(\omega)$ could, in principle, be calculated in the standard manner that elastic stiffness matrices are calculated, but using the complex material properties evaluated at frequency ω rather than the corresponding elastic material properties.

- It is a result of classical linear viscoelasticity that K_o above, is the stiffness matrix that would be constructed using material properties obtained from quasistatic measurements [5].

- The vectors x^n and z^n form a biorthogonal set:

$$(x^k)^T\, z^l = \delta_{kl} \tag{2.8}$$

The above relationship was central to the derivation of [4].

- The elastic eigenmodes, x^k, are determined at this point only up to an arbitrary factor. They become uniquely defined when scaled so that

$$(x^k)^T\, M\, x^k = 1 \tag{2.9}$$

for each mode k. This is one of the standard forms of eigenvector normalization and from substitution of the above equation into Equation 2.3, the eigenfrequencies can be isolated:

$$(x^k)^T f^k = (\omega^k)^2 \tag{2.10}$$

This normalization becomes useful below in the extraction of complex eigenpairs for the damped system.

- Though the damping and stiffness matrices (Equations 2.1 and 2.2) of Equation 2.7 are expressed as expansions involving x^n and ω^n, these are eigensolutions of the elastic problem, Equation 2.3, and not of the damped system, Equation 2.7.
- The matrices defined by Equations 2.1 and 2.2 are, in general, full and non-symmetric. Though at first disconcerting, these features should not be unexpected: symmetric damping and stiffness matrices should be expected only where there exist elastic strain energies and Rayleigh dissipation functions. Such potentials do not exist for general viscoelastic materials.

Elastic Modal Coordinates

In order to deal with a smaller system of equations, it is useful to express displacements in terms of the elastic modal coordinates:

$$x(t) = \sum_{\text{modes } n=1}^{N} \alpha^n(t)\, x^n \tag{2.11}$$

(The modal coordinates $\alpha^n(t)$ are found by contracting the above equation with $(z^k)^T$ and invoking Equation 2.8 to obtain the following:)

$$\alpha^n(t) = (z^n)^T x(t) \tag{2.12}$$

Premultiplication of Equation 2.7 by $(x^k)^T$ and substitution of Equation 2.11 for $x(t)$, generates the system equations in terms of the elastic modal coordinates.

$$\hat{I}\,\ddot{\alpha}(t) + \hat{C}\,\dot{\alpha}(t) + \hat{K}\,\alpha(t) = \beta(t) \tag{2.13}$$

In the above, the vector $\alpha(t)$ is composed of the scalars $\alpha^n(t)$, $\hat{I}$ is the N'th order identity matrix, and the matrices $\hat{C}$ and $\hat{K}$ are defined by

$$\hat{C}_{k,l} = (x^k)^T h^l \tag{2.14}$$

and

$$\hat{K}_{k,l} = (x^k)^T g^l \tag{2.15}$$

where

$$h^k = Im\left(\frac{1}{\omega^k} \Gamma^*(\omega^k) \right) x^k \tag{2.16}$$

and

$$g^k = Re\left(\Gamma^*(\omega^k) \right) x^k \tag{2.17}$$

The components, $\beta^n(t)$, of the vector $\beta(t)$ are the contraction of $r(t)$ with each of the elastic eigenmodes:

$$\beta^n(t) = (x^n)^T r(t) \tag{2.18}$$

It should be noted that the equations of [2] and [3] result if all off-diagonal terms of Equation 2.14 for $\hat{C}$ are dropped and the term g^l in Equation 2.15 for $\hat{K}$ is replaced by f^l. Such a reduction of Equations 2.14 and 2.15 to obtain those of [2] and [3] is reflective of that method's assumptions that elastic eigenmodes are preserved and that strain energy is independent of frequency.

Frequency Response Matrices and Complex Eigenanalysis

Once the matrices $\hat{C}$ and $\hat{K}$ have been calculated, Equation 2.13 is recast as a first order system of equations in state space and the complex eigenmodes and frequencies are extracted. We have chosen to use the formalism of Newland [6] for these steps of the calculation. Letting

$$s(t) = \left\{ \begin{array}{c} \alpha(t) \\ \dot{\alpha}(t) \end{array} \right\} \tag{2.19}$$

Equation 2.13 becomes

$$\dot{s}(t) = A\, s(t) + F(t) \tag{2.20}$$

where

$$A = \left[\begin{array}{cc} 0 & \hat{I} \\ -\hat{K} & -\hat{C} \end{array} \right] \tag{2.21}$$

and

$$F(t) = \left\{ \begin{array}{c} 0 \\ \beta(t) \end{array} \right\} \tag{2.22}$$

The above state-space equation is diagonalized through introduction of a matrix, U, whose columns are the complex right-eigenvectors of A:

$$A\,U = U\,\Lambda \tag{2.23}$$

where Λ is a matrix whose diagonal terms are the complex eigenvalues, λ_k, of A and whose off-diagonal terms are zero. Since A is a $2N$ by $2N$ matrix, U and Λ are also of dimension $2N$. Both U and Λ are products of standard numerical eigensolvers.

Each complex eigenpair, (U_k, λ_k) and its conjugate, (U_k^*, λ_k^*) combine to generate real displacements:

$$s(t) = D\, e^{\mu_k t}\, [\cos(\psi_k t + \theta)\; Re\,(U_k) \;-\; \sin(\psi_k t + \theta)\; Im\,(U_k)] \tag{2.24}$$

where $\mu_k = Re\,\lambda_k$ is the damping factor for that mode, $\psi_k = Im\,\lambda_k$ is the damped natural frequency for that mode, and D and θ are indeterminate. The above expression transforms, through Equations 2.11 and 2.19, to corresponding expressions in terms of displacement coordinates:

$$x(t) = D\, e^{\mu_k t} \sum_{modes\ n=1}^{N} x^n\, [\cos(\psi_k t + \theta)\; Re\,(U_k^n) \;-\; \sin(\psi_k t + \theta)\; Im\,(U_k^n)] \tag{2.25}$$

and

$$\dot{x}(t) = D\, e^{\mu_k t} \sum_{modes\ n=1}^{N} x^n\, \left[\cos(\psi_k t + \theta)\; Re\,\left(U_k^{N+n}\right) \;-\; \sin(\psi_k t + \theta)\; Im\,\left(U_k^{N+n}\right)\right] \tag{2.26}$$

where U_k^n is the n'th component of the k'th complex eigenmode. From the above, it is seen that when expressed in spatial coordinates, the k'th complex eigenmode, x_c^k, is:

$$x_c^k = \sum_{modes\ n=1}^{N} x^n\, U_k^n \tag{2.27}$$

The complex frequency λ_k can also be expressed in the more common terms of damping ratio ξ_k and a nominal "undamped" frequency $\hat{\omega}^k$:

$$\lambda_k = \hat{\omega}^k \left[-\xi_k \;+\; i\sqrt{1 - \xi_k^2}\right] \tag{2.28}$$

where

$$\xi_k = \sqrt{\frac{(Re\,\lambda_k)^2}{(Re\,\lambda_k)^2 + (Im\,\lambda_k)^2}} \tag{2.29}$$

and

$$\hat{\omega}^k = -Re\,\lambda_k / \xi_k \tag{2.30}$$

In general, the nominal "undamped" frequency $\hat{\omega}^k$ will not equal any of the natural frequencies of the underlying elastic system, since the complex modes do not, in general, equal any individual elastic mode.

Equation 2.23 is substituted into Equation 2.20 and the result is rearranged to yield an uncoupled system of equations which can be integrated to yield $s(t)$:

$$s(t) = U\, e^{\Lambda t}\, s(0) \;+\; U \int_0^t e^{\Lambda (t-\tau)}\, U^{-1}\, F(\tau)\, d\tau \tag{2.31}$$

The quantity $e^{\Lambda t}$ is the diagonal matrix of terms $e^{\lambda_k t}$.

In the case of harmonic excitation forces,

$$F(t) = Re\left\{ \begin{array}{c} 0 \\ \beta_0 e^{i\omega t} \end{array} \right\} \tag{2.32}$$

Equation 2.31 becomes

$$s(t) = Re\left(\hat{H}(\omega)\left\{ \begin{array}{c} 0 \\ \beta_0 e^{i\omega t} \end{array} \right\}\right) \tag{2.33}$$

where $\hat{H}(\omega)$ is the frequency response matrix

$$\hat{H}(\omega) = U\ d(\omega)\ U^{-1} \tag{2.34}$$

and

$$d(\omega) = \left[\begin{array}{ccc} \frac{1}{i\omega-\lambda_1} & 0 & 0 \\ 0 & \ddots & 0 \\ 0 & 0 & \frac{1}{i\omega-\lambda_{2N}} \end{array} \right] \tag{2.35}$$

Since $\hat{H}$ is constructed from the eigenvectors and eigenvalues of A, and those eigenquantitites occur in complex conjugate pairs, it is not surprising that there is some redundant information in $\hat{H}$. Only the upper right-hand quarter of $\hat{H}(\omega)$,

$$\hat{H}^{1,2}(\omega) = \hat{P}\ d(\omega)\ \hat{Q} \tag{2.36}$$

where $\hat{P}$ is the upper half of U and $\hat{Q}$ is the right half of U^{-1}, is necessary for calculating the displacement frequency response of the structure

$$\alpha(t) = Re\ \left(\hat{H}^{1,2}(\omega)\,\beta_0\, e^{i\omega t}\right) \tag{2.37}$$

Substitution of Equation 2.18 into Equation 2.37 and substitution of the result into Equation 2.11 returns the frequency response matrix for the original displacement vector $x(t)$:

$$x(t) = Re\ \left(H(\omega)\, r_0\, e^{i\omega t}\right) \tag{2.38}$$

where

$$H(\omega) = P\, d(\omega)\, Q \tag{2.39}$$

and

$$P_{i,k} = \sum_{modes\ n=1}^{N} x_i^n\, \hat{P}_{n,k} \tag{2.40}$$

and

$$Q_{k,j} = \sum_{\text{modes}\ n=1}^{N} \hat{Q}_{k,n}\, x_j^n \tag{2.41}$$

Evaluation of individual components $H_{i,j}(\omega)$ over ranges of ω involves far fewer calculations than would first appear since only individual rows of P and individual columns of Q need to be evaluated and stored while the diagonal matrix $d(\omega)$ is evaluated over the frequency range of interest.

2.2 Numerical Implementation

There are two parts to the numerical implementation of the formulation developed above:

- the evaluation of the damping and stiffness matrices occurring in Equation 2.13.
- the matrix operations associated with evaluation of complex modes and frequencies and the calculation of the frequency response matrix.

Evaluation of Damping and Stiffness Matrices

Evaluation of $\hat{C}$ and $\hat{K}$ is done through the following steps:

1. Material properties for all constituent materials are tabulated – as functions of frequency – in two distinct sets of tables: one for storage response (real part) and one for loss response (imaginary part). (With the finite element code used in this project, MSC NASTRAN [7], it is convenient to use the table formats which that code associates with temperature-dependent material properties.) For the second set of tables, the loss moduli are divided by ω so that it is actually viscosity type properties that are tabulated.

   It is important that the tabulated material properties are tailored so that Lame' constants calculated from them are the real and imaginary parts of the Lame' constants of the material.

2. NASTRAN is used to formulate and solve the elastic eigenproblem of Equation 2.3. In this step, the stiffness matrix is constructed from the real part of the material response in the limit of zero frequency. This step generates quantities ω^n and x^n for the range of frequencies of interest.

   NASTRAN is also used to evaluate h^n and g^n (Equations 2.16 and 2.17). For each eigenpair (ω^n, x^n), two statics problems are directed to NASTRAN

(a) for which the displacements are specified as x^n and the material properties are selected from the first set of tables and evaluated at frequency ω^n. The resulting force vector is g^n.

(b) for which the displacements are specified as x^n and the material properties are selected from the second set of tables and evaluated at frequency ω^n. The resulting force vector is h^n.

The above calculations are done with procedures which are documented in the MSC literature for the solution of problems involving temperature dependent material properties.

3. $\hat{C}$ and $\hat{K}$ are evaluated in the manner indicated in Equations 2.14 and 2.15, by taking inner products of vectors x^k with vectors g^l and h^l, respectively. The appropriate Fortran coding is reasonably straightforward.

Complex Modes and Frequencies, Damping Ratio, and Frequency Response

1. Matrix A of Equations 2.21 is constructed in the manner indicated, and its complex eigensolutions are extracted using routines found in the SLATEC [8] library of Fortran code. Some sorting and normalization of the complex eigenvectors U_k is useful before printing. (In the case that the n'th elastic eigenmode is preserved, the associated complex eigenvector is zero in all but the n'th and $N+n$'th components.) Damping ratios for each complex mode are calculated from Equation 2.29 and printed along with the corresponding complex eigenfrequency-eigenmode pair.

2. Fortran code has also been written along the lines suggested by Equations 2.39 through 2.41 for the evaluation of complex frequency response functions for given nodal-force/nodal-displacement pairs.

The above codes generate three quantities that can be compared to experiment: complex mode shape, complex frequency (including damping ratio), and frequency response functions.

Also, though it cannot be demonstrated in this media, Fortran code has been written to evaluate Equation 2.25 to generate Patran [9] ".DIS" files which are then used to create movies of the complex modes.

3. The Experiment

AFWL/ARBC personnel performed experimental modal surveys on two test articles in support of this verification effort. The test articles were residual hardware from a previous study on damping techniques [10]. The first test article was a 68" x 2" x 1/8" aluminum C-channel extrusion. The second test article was an identical C-channel extrusion treated with constrained layer damping. This treatment which was applied to the backside of the beam, consisted of a layer of viscoelastic material(VEM), 3M ISD-112, sandwiched between the beam surface and an aluminum constraining layer (see Figure 3.1). Elastic properties for the aluminum and for the polymer are provided in Table 3.1 and the viscoelastic properties of the polymer are provided in Tables 3.2 and 3.3. The test articles were suspended using elastic bands at the two ends to simulate free-free boundary conditions in the modal testing.

This test utilized an Endevco model 23 triaxial accelerometer to measure motion of the test article and an instrumented impact hammer to apply and measure the input disturbance. The Endevco model 23 triaxial accelerometer is a very lightweight piezoelectric motion sensor, and was chosen to avoid mass-loading issues, particularly in the testing of the undamped beam. The outputs of this device were attached to three B & K model 2635 charge amplifiers, which convert the accelerometer output to a voltage and perform signal amplification. The input disturbance was provided by a PCB model 086B03 impact hammer. This hammer has a force gage built into the tip which measures the input disturbance. The output of this gage was attached to a PCB model 480D06 power unit which amplified the sensor signal.

This amplified input signal and the three charge amplifier output signals were input to the first four channels of the data acquisition system. The Modal Analysis Data Reduction And Testing System (MADRATS) was the primary testing computer for this program. This system is based on a Hewlett Packard A-900 computer, a multi-user, real-time interrupt system. This system includes a 132 Mbyte hard disk, 3 Mbyte memory and a complete data acquisition and analysis workstation. The system also includes other support peripherals such as printers, plotters, and tape drives.

The system front end is a 64 channel DIFA SCADIS data acquisition system. The DIFA SCADIS is fully programmable, either manually from the attached keypad or through the data acquisition software on the computer via an HP-IB interface. This front end utilizes programmable gain pre-filter and post-filter amplifiers and programmable bandpass filters. The SCADIS samples all channels in parallel using sample and hold buffers. This data is digitized by the SCADIS and then multiplexed into the

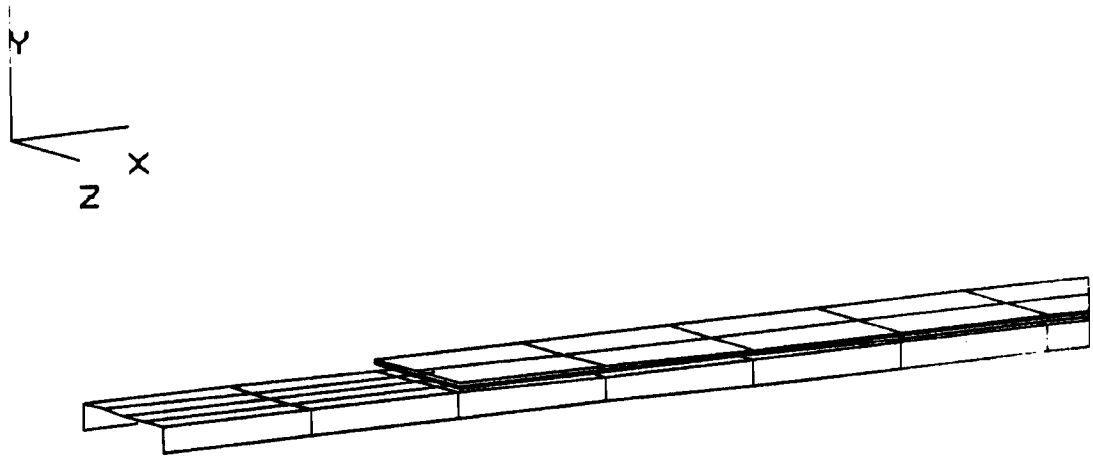

Figure 3.1. Left edge of aluminum beam with damping treatment, illustrating finite element meshing.

Material	Shear Modulus G_0 (psi)	Poisson'c Ratio	Density (lb sec^2/in^4)
Aluminum	3.76E6	0.33	2.54E-4
3M ISD-112	60.0	0.49	1.90E-4

Table 3.1. Elastic Properties of Aluminum and 3M ISD-112

A-900 computer memory via a parallel interface. This system has a frequency range of 0.1 to 10,000 Hz and a dynamic range of 63 dB. The maximum throughput rate to memory of the SCADIS is 350 kHz.

Data acquisition is accomplished through the Leuven Measurement Systems Fourier Monitor (FMON) software package. Several modal testing techniques can be performed using FMON, including forced response, power spectrum, and impact testing. Testing can be set up and performed using menu-driven programs, user-defined command stacks or manually. The test program covered in this report utilized the menu-driven programs which allow test setups to be stored into and loaded from memory. Test setups from memory were used, requiring changes only to transducer location for the various test runs.

Data reduction is also performed on the MADRATS computer using the Leuven Measurements Systems Super Modal Analysis Package (SMAP). SMAP computes the modal parameters of a structure from the frequency response functions produced in data acquisition. This software package has several available parameter estimation techniques to tailor analysis to a specific test. The primary algorithm used in reducing the data of this test program was the Least Squares Complex Exponential Time Domain Method. In addition, a variety of curve fitters are available, including a real and imaginary fitter, circle fitters, and a Least Squares multiple degrees of freedom fitter. The least squares MDOF method was the most frequently used because of the modal density involved in these tests. The specific applications of these methods will be discussed in more detail in the Results section of this report.

The first tests were performed on the bare beam. Prior to testing, a test setup file was generated and stored on the computer. The testing consisted of a 200 Hz bandwidth, roving accelerometer impact test. The accelerometer was first attached to the beam, and the point number and direction information was entered into the computer. The structure was tapped by the impact hammer at a point at one end of the beam, 0.5 inches from the centerline, in order to perform the autoranging of the data acquisition channel amplifiers. A series of eight impacts was performed, and the data was averaged and processed to provide frequency response and coherence functions for each of the three axes at the data point. The power spectra of each impact, and the frequency response functions for the response channels were each viewed prior to

acceptance, and the resulting transfer functions were stored on the disk. This procedure was repeated for each of the 36 data points on the bare beam, and for the 36 data points on the damped beam whose data was stored under a different test identification.

The frequency response functions for the undamped beam exhibited high amounts of spectral leakage, leading to poor coherence functions. Exponential windowing was used on the response data for the undamped beam to reduce the leakage to acceptable levels. This added damping by the window can be backed out of the modal parameters calculated from data reduction. Windowing was not required or used in testing the damped beam because the higher damping exhibited by this structure greatly reduced leakage effects.

Storage Modulus $G'(f) = G_0 * (1.0 + g(f))$					
frequency f (hz)	$g(f)$	frequency f (hz)	$g(f)$	frequency f (hz)	$g(f)$
.00E+00	.00E+00	.70E+01	.18E+00	.31E+02	.68E+00
.13E+03	.19E+01	.40E+03	.46E+01	.14E+04	.11E+02
.46E+04	.24E+02	.14E+05	.58E+02	.55E+05	.12E+03
.20E+06	.24E+03	.13E+07	.46E+03	.40E+07	.62E+03
.22E+08	.81E+03	.87E+08	.98E+03	.49E+09	.12E+04
.18E+10	.13E+04	.54E+10	.15E+04	.22E+11	.16E+04
.39E+11	.17E+04				

Table 3.2. Storage Modulus of 3M ISD-112

Loss Modulus $G''(f) = 2\pi f * G_0 * h(f)$					
frequency f (hz)	$h(f)$	frequency f (hz)	$h(f)$	frequency f (hz)	$h(f)$
.00E+00	.23E-01	.23E+01	.16E-01	.67E+01	.11E-01
.21E+02	.81E-02	.42E+02	.65E-02	.11E+03	.46E-02
.24E+03	.35E-02	.49E+03	.29E-02	.65E+03	.25E-02
.13E+04	.19E-02	.31E+04	.14E-02	.96E+04	.84E-03
.28E+05	.49E-03	.64E+05	.30E-03	.25E+06	.11E-03
.14E+07	.22E-04	.77E+07	.39E-05	.46E+08	.66E-06
.33E+09	.93E-07	.24E+10	.12E-07	.11E+11	.25E-08
.41E+11	.63E-09	.54E+11	.46E-09		

Table 3.3. Loss Modulus of 3M ISD-112

4. Experimental Results and Comparison with Experiment

Figure 4.1 shows the driving point frequency response functions for the two beams. The driving point is at one end of the beam, 0.5 inches from the center line. The sharpness in the peaks of the bare beam transfer function graphically demonstrate the extremely low damping present in this beam. The shorter, more rounded peaks in the frequency response function of the damped beam demonstrate graphically the effect of the treatment both on the damping present in the beam and the magnitude of response at the natural frequencies. These frequency response functions also demonstrate a slight frequency shift due to the increased stiffness provided by the damping treatment. Frequency response functions similar to the driving point response function were stored on the disk for each data point on the two beams.

Data reduction was performed using the Super Modal Analysis Package (SMAP) software residing on MADRATS. The data was reduced using a Least Squares Exponential method for parameter estimation and curve fitting. This data reduction resulted in modal frequency and damping information, as well as displacement files for each mode of the structure in the 0-200 Hz bandwidth. This procedure was repeated for the data sets for each beam. Table 4.1 shows a comparison of the results from the two test articles in terms of frequency and damping.

Figure 4.2 is a series of plots for the mode shapes of the damped beam. These mode shapes were produced by combining the displacement files produced by the data reduction with a geometry file. This data can also be animated to aid in the interpretation of the mode shapes.

The damping results for the final mode were not included because they were somewhat suspect. To prevent aliasing in the data, the data acquisition system filters were set to roll off at 70% of the upper frequency of a test. This last mode was so close to the upper frequency bound that most of its signal was likely below the noise floor, making it impossible for the parameter estimator to determine the damping values. This mode was retained simply as another frequency value for comparison with the analytic results.

The results of the analytic modeling and experimental testing were compared in three ways. First, a qualitative comparison was drawn between the frequency response functions developed analytically and through testing. Figure 4.3 shows an overlay of the experimental and analytic driving-point frequency response functions for the damped beam. The dashed curve is the experimental data. The impact hammer used to excite

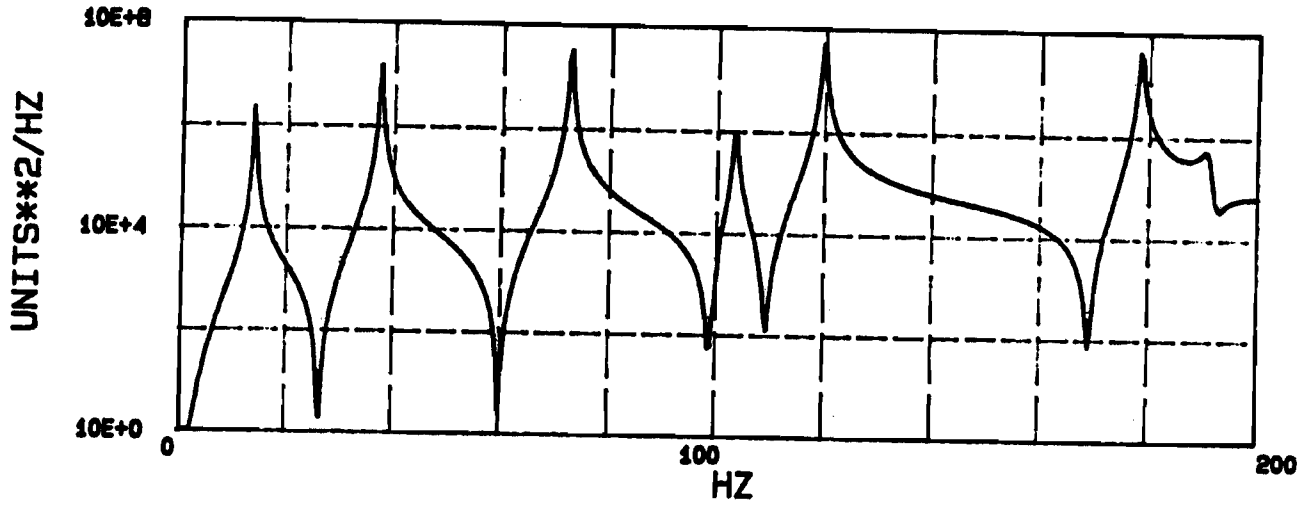

(a) Frequency Response Function of Undamped Beam.

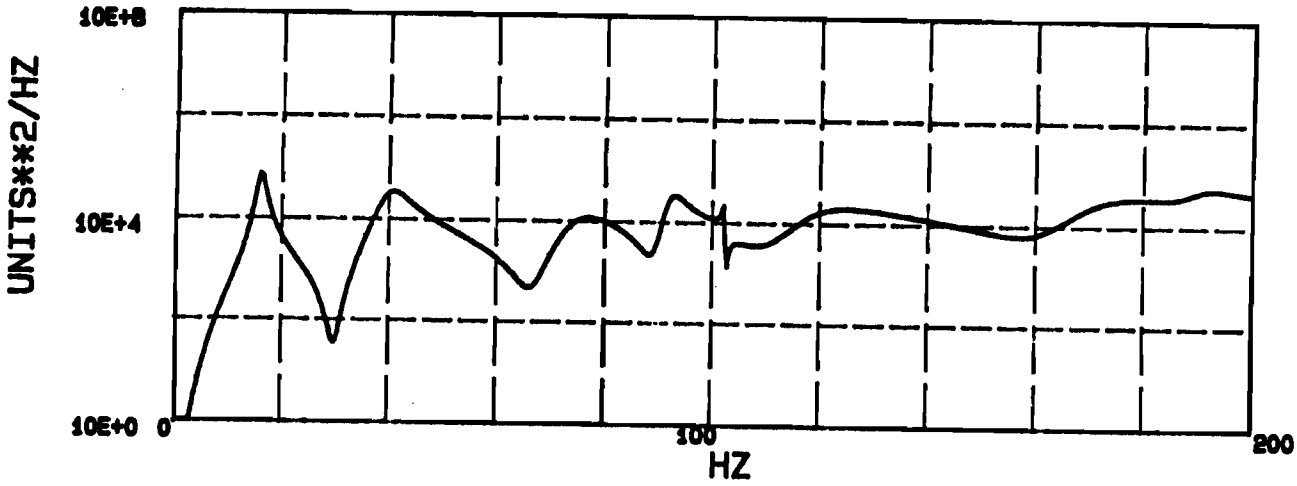

(b) Frequency Response Function of Damped Beam.

Figure 4.1. Driving point frequency response of damped and undamped beams

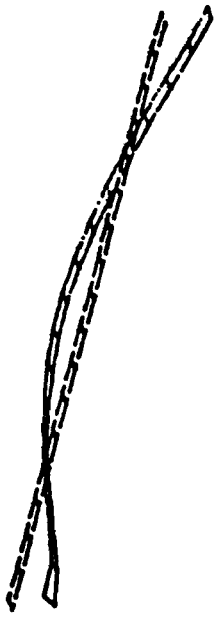

f_1 = 15.68 Hz
1st Bending

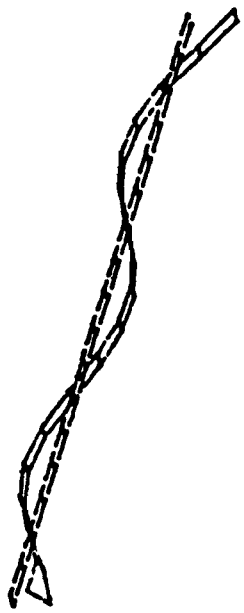

f_2 = 39.78 Hz
2nd Bending

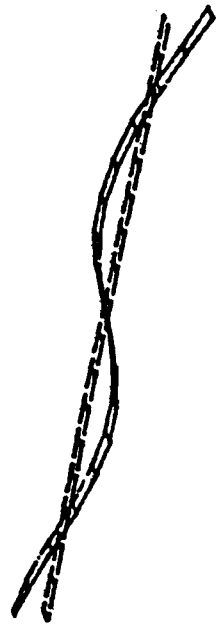

f_3 = 73.76 Hz
3rd Bending

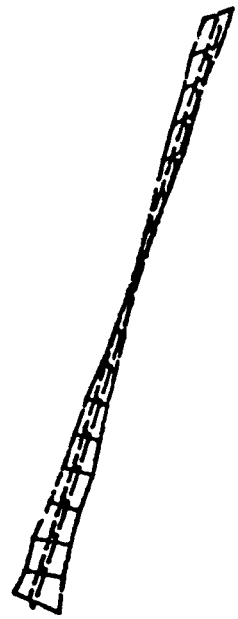

f_4 = 91.81 Hz
1st Torsional

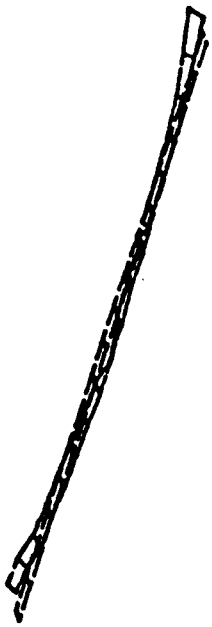

f_5 = 101.9 Hz
1st Bending (in-plane)

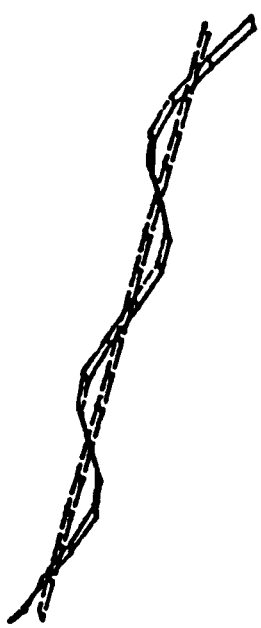

f_6 = 116.5 Hz
4th Bending

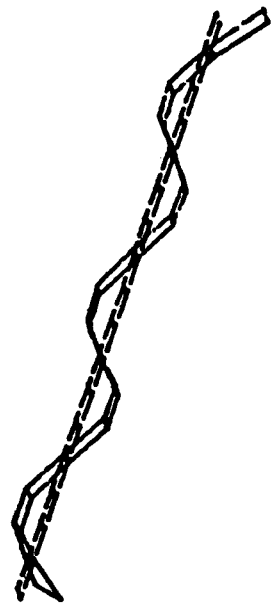

f_7 = 169.6 Hz
5th Bending

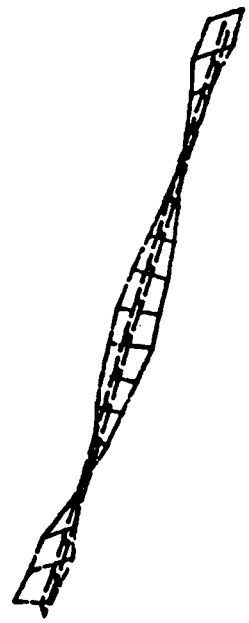

f_8 = 190.0 Hz
2nd Torsional

Figure 4.2. Real and Imaginary components of complex modes of damped beam. Imaginary components are essentially zero.

Mode	Undamped Beam		Damped Beam	
	Frequency (Hz)	Damping (% Critical)	Frequency (Hz)	Damping (% Critical)
1st Bending	13.38	0.295	15.68	5.837
2nd Bending	37.00	0.190	39.78	8.069
3rd Bending	72.12	0.156	73.76	8.489
1st Bending (in-plane)	99.77	0.278	101.95	0.204
1st Torsional	102.90	0.289	91.81	2.386
4th Bending	119.13	0.211	116.46	8.367
5th Bending	177.84	0.146	169.63	7.054
2nd Torsional	190.58	—	190.01	—

Table 4.1. Experimental Test Results

the experimental modes was uncalibrated, so the experimental curve is known only up to a multiplicative constant, corresponding to a vertical translation in the semi-log plot shown here.

Comparison of the frequency and damping information from the test data and modeling results provides a more quantitative method of comparison. Tables 4.2 and 4.3 contain these results for the two test articles. Note that both prediction and experiment for the damped beam show a reordering of the first torsional and the first in-plane-bending modes.

The comparison of the first test article results was used to gain confidence in the NASTRAN model of the beam prior to modeling the damping treatment. As one can see from the results presented in this table, nearly identical results were achieved through testing and modeling of the undamped beam, particularly in the bending modes. The larger differences in the natural frequency values for the two torsional modes have been attributed to fundamental torsional characteristics of the plate elements used in the modeling.

The second test article was compared using damping as well as natural frequency results. As indicated in the table, the frequency values are again nearly identical, with the largest variance being less than seven percent, and all of the bending modes being within five percent. The damping results were not predicted as well as the frequencies, but this is expected considering the relative difficulties in both measurement and prediction. The agreement between measured and predicted damping values is encouraging since they agree to within the uncertainty of viscoelastic properties of the polymer.

The difference for the in-plane bending mode damping was the highest, but it is

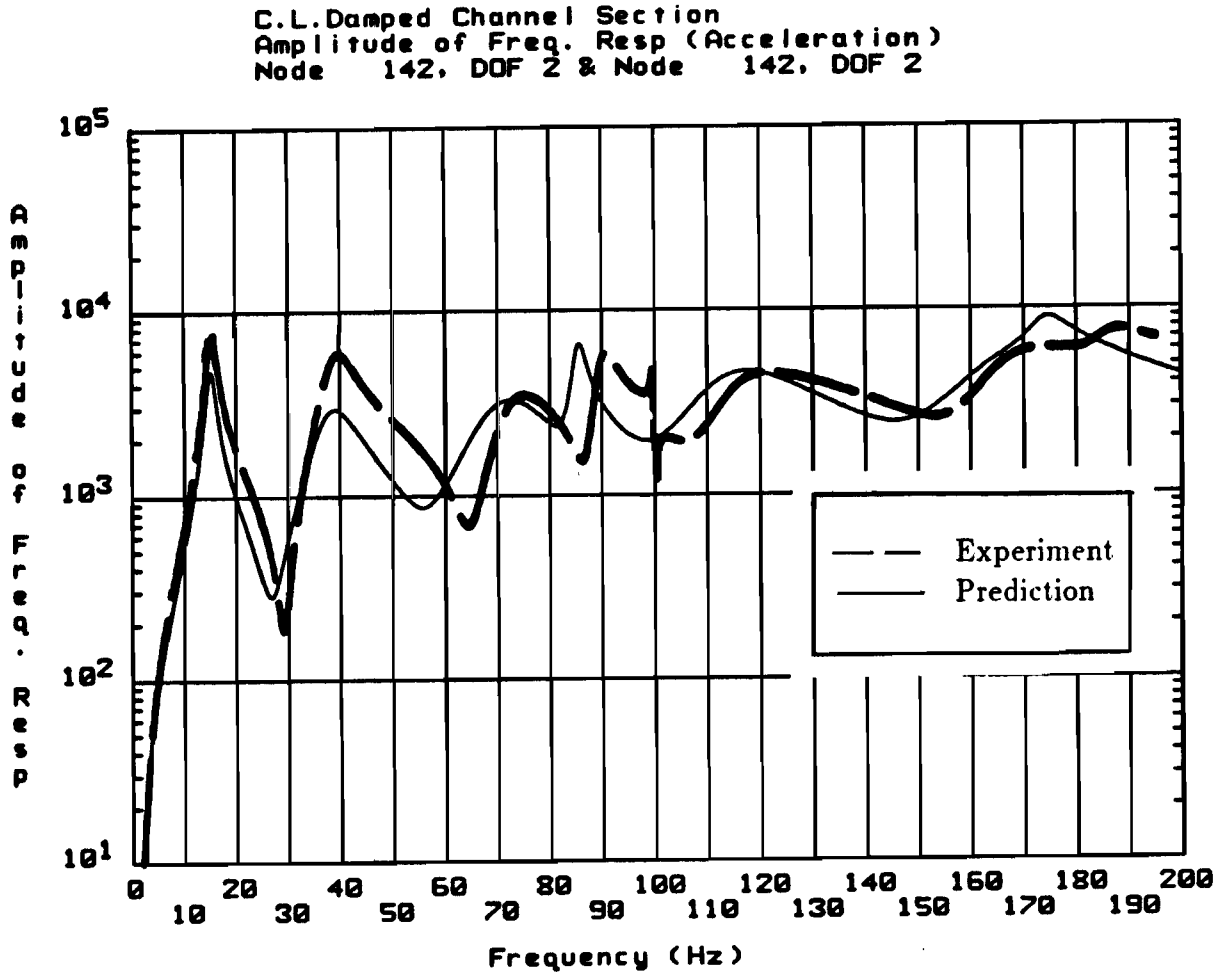

Figure 4.3. Overlay of the experimental and analytic frequency response functions for the damped beam. The dashed curve is the experimental data.

Mode	AFWL Measured Frequency (Hz)	Sandia Predicted Frequency (Hz)	% Diff.
1st Bending	13.38	13.75	2.7
2nd Bending	37.00	37.82	2.2
3rd Bending	72.12	74.01	2.6
1st Bending (in-plane)	99.77	100.70	0.9
1st Torsional	102.90	85.40	18.6
4th Bending	119.13	122.10	2.5
5th Bending	177.84	182.10	2.4
2nd Torsional	190.58	173.10	9.6

Table 4.2. Comparison of Undamped Beam Results

Mode	AFWL Measured		Sandia Predicted		% Diff.	
	Freq. (Hz)	Damp. (% Cr.)	Freq. (Hz)	Damp. (% Cr.)	Freq.	Damp.
1st Bending	15.7	5.8	15.1	6.1	3.9	5.0
2nd Bending	39.8	8.1	38.0	11.3	4.6	33.0
3rd Bending	73.8	8.5	70.6	12.0	4.4	34.1
1st Torsional	91.8	2.4	87.2	1.7	5.1	34.1
1st Bending (in-plane)	102.0	0.2	102.6	0.07	0.6	96.3
4th Bending	116.5	8.4	113.4	10.2	2.7	19.4
5th Bending	169.6	7.1	166.8	9.2	1.7	25.8
2nd Torsional	190.0	—	177.5	2.6	6.8	—

Table 4.3. Comparison of Damped Beam Results

important to note that the experimentally measured result is highly suspect due to the difficulty in imposing a purely vertical impulse at the driving point.

A method known as Modal Assurance Criterion (MAC) was also used in comparing the analytic and experimental results. MAC is a least squares approach to determining the consistency of estimated modal vectors of a system. MAC is calculated using the equation:

$$\mathrm{MAC}_{m,n} = \left|(x_c^m)^T (y_c^n)^*\right|^2 / [(x_c^m)^T (x_c^m)^* \; (y_c^n)^T (y_c^n)^*] \tag{4.1}$$

where x_c^m is an estimate (in this case numerical) for the m'th complex eigenmode and

y_c^n is an estimate (in this case experimental) for the n'th complex eigenmode. A little algebra will verify that

$$1 - \mathrm{MAC}_{m,n} = \frac{1}{(x_c^m)^T (x_c^m)^*} \min_{\alpha} |x_c^m - \alpha\, y_c^n|^2 \tag{4.2}$$

MAC is a scalar constant between 0 and 1 relating the two modal vectors. (It may be thought of as the square of the cosine between those vectors.) A MAC value of one or nearly one will give confidence that the modal vectors represent the same modes. If the MAC value is near zero, there is no linear relationship between the two estimates, indicating two different modal vectors.

The eight experimental and eight analytic modal vectors were compared using the MAC procedure. The results of this comparison are shown in Figure 4.4. The blocked-in area of the chart indicates the results when the similar analytic and experimental vectors were compared. These results, particularly the out-of-plane bending modes, give confidence that these modal vectors describe the same mode, and are nearly identical.

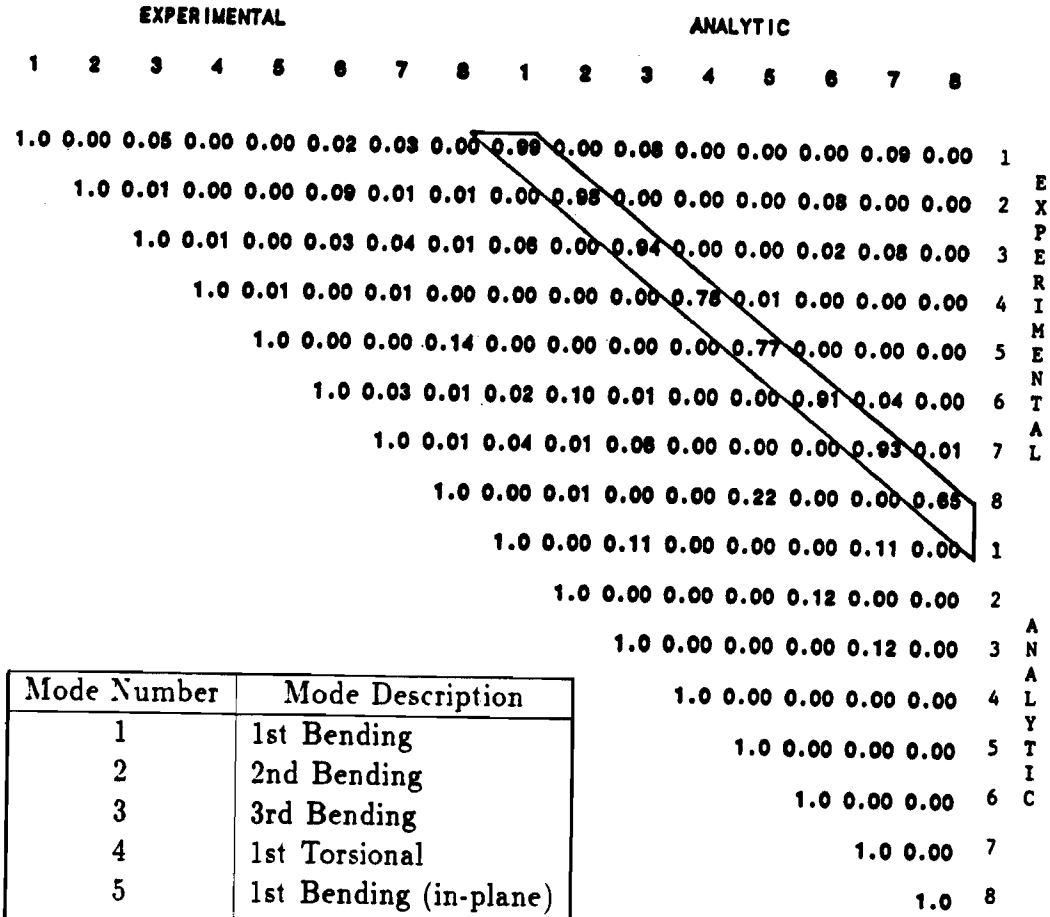

Mode Number	Mode Description
1	1st Bending
2	2nd Bending
3	3rd Bending
4	1st Torsional
5	1st Bending (in-plane)
6	4th Bending
7	5th Bending
8	2nd Torsional

Figure 4.4. MAC parameters of experimental and analytic modal vectors for first eight complex modes.

5. Conclusions

Though the structure employed in this study was very simple, this study does demonstrate the predictive capability of the computational method of reference [4]. Though the structure had sufficient symmetries to preclude the existence of true complex modes, it did have sufficient character in its frequency response functions and damping parameters to permit some comparison of the desired sort.

Particularly encouraging was that the predicted and measured damping values for the beam agree to within the uncertainty of the viscoelastic properties of the damping polymer.

The study served its purpose in providing sufficient confidence in both the numerical and experimental methods to facilitate future studies involving more sophisticated structures.

Some further comments about the computational process are appropriate:

- Though the numerical implementation of the derivations of the second chapter of this report did require writing much original computer code, the onerous work of involving mesh generation, finite element eigen- and static analysis was done with the aid of the commercial codes PATRAN and MSC-NASTRAN.
- With the exception of the finite element analysis, the calculations can be performed with reasonably small matrices. This is achieved by using the elastic modes as generalized coordinates and restricting attention to the frequency range of interest.
- The complex modes can be assembled in a systematic manner from the mass, damping, and stiffness matrices using the formalism of Newland [6]. The complex modes can then be used, in the manner shown here, to calculate transient response (Equation 2.31) and frequency response (Equation 2.38).

References

[1] D. Ross, E. E. Ungar, and E. M. Kerwin, "Damping of plate flexural vibrations by means of viscoelastic laminae", *Structural Damping*, ASME, New York, pp. 49-87.

[2] C. D. Johnson and David Kienholz, "Finite element prediction of damping in structures with constrained viscoelastic layers", *AIAA Journal*, Vol 20, September 1982, pp. 1284-1290.

[3] C. D. Johnson, D. A. Kienholz, and L. C. Rogers, "Finite element prediction of damping in beams with constrained viscoelastic layers", *Shock Vib. Bull.*, Vol. 51, Pt. 1, May 1981, pp. 71-81.

[4] D. J. Segalman, "Calculation of damping matrices for linearly viscoelastic structures", *Journal of Applied Mechanics*, Vol. 109, September 1987, pp. 585-588.

[5] J. D. Ferry, *Viscoelastic Properties of Polymers*, (Third Edition) John Wiley and Sons, New York, 1980, p. 68, Equations 39 and 40.

[6] D. E. Newland, "On modal analysis of non-conservative linear systems", *Journal of Sound and Vibration*, Vol. 112, 1987, pp. 69-96.

[7] *MSC/NASTRAN Users' Manual: MSC/NASTRAN Version 64*, MacNeal-Schwendler Corporation, Los Angeles, May 1976.

[8] W. H. Vandevender, "The Slatec mathematical subprogram library version 2.0", SAND84-281, April 1984.

[9] *PATRAN Plus Users Manual*, PDA Engineering, Costa Mesa, CA., 1987, Chapter 27, p. 130.

[10] Kevin Smith, CSA Engineering Report No. 87-04-02, "Damping of a selected structure", April 1987.